10-1-2020

Ultrawideband Frequency-Selective Absorber Designed with an Adjustable and Highly Selective Notch

Yuxuan Ding
Communication University of China

Mengyao Li
Communication University of China

Jianxun Su
Communication University of China

Qingxin Guo
Communication University of China

Hongcheng Yin
Communication University of China

See next page for additional authors

Ultrawideband Frequency-Selective Absorber Designed with an Adjustable and Highly Selective Notch

Abstract

In this paper, the working mechanism of a wideband absorber designed with an adjustable and highly selective notch band is studied, in which the narrow notch band is independently controlled by the lower lossless layer of the absorber, while the upper lossy layer loaded with lumped resistors realizes absorption. We present two instances with geometrically controlled and electrically controlled notch bands, respectively. Without decreasing absorption performance, the notch position can be flexibly adjusted throughout the entire frequency band by simply modifying the dimension of the lossless frequency-selective surface (FSS) or changing the capacitance of the varactor, i.e., using geometric control or electrical control. The narrow notch band allows two wide absorption bands to be retained on both sides; therefore, good stealth performance is still guaranteed. Equivalent circuit models (ECM) are proposed to further explain the principle. The frequency-domain simulation, ECM, time-domain simulation, and experimental results are in good agreement and validate the adjustability and high selectivity of the notched absorbers. At the end of this paper, an FSA-backed monopole antenna is simulated and measured, which clearly illustrates that these FSAs can serve as the ground plane for antennas and realize out-of-band RCS reduction.

Keywords

tunable notch, frequency-selective absorber (FSA), RCS reduction, equivalent circuit model (ECM)

Disciplines

Signal Processing | Systems and Communications

Comments

This is a manuscript of an article published as Ding, Yuxuan, Mengyao Li, Jianxun Su, Qingxin Guo, Hongcheng Yin, Zengrui Li, and Jiming Song. "Ultrawideband Frequency-Selective Absorber Designed with an Adjustable and Highly Selective Notch." *IEEE Transactions on Antennas and Propagation* (2020). DOI: 10.1109/TAP.2020.3026889. Posted with permission.

Authors

Yuxuan Ding, Mengyao Li, Jianxun Su, Qingxin Guo, Hongcheng Yin, Zengrui Li, and Jiming Song

Ultrawideband Frequency-Selective Absorber Designed with an Adjustable and Highly Selective Notch

Yuxuan Ding, Mengyao Li, Jianxun Su, *Member, IEEE*, Qingxin Guo, *Senior Member, IEEE*, Hongcheng Yin, Zengrui Li, *Member, IEEE*, and Jiming Song, *Fellow, IEEE*

***Abstract*—In this paper, the working mechanism of a wideband absorber designed with an adjustable and highly selective notch band is studied, in which the narrow notch band is independently controlled by the lower lossless layer of the absorber, while the upper lossy layer loaded with lumped resistors realizes absorption. We present two instances with geometrically controlled and electrically controlled notch bands, respectively. Without decreasing absorption performance, the notch position can be flexibly adjusted throughout the entire frequency band by simply modifying the dimension of the lossless frequency-selective surface (FSS) or changing the capacitance of the varactor, i.e., using geometric control or electrical control. The narrow notch band allows two wide absorption bands to be retained on both sides; therefore, good stealth performance is still guaranteed. Equivalent circuit models (ECM) are proposed to further explain the principle. The frequency-domain simulation, ECM, time-domain simulation, and experimental results are in good agreement and validate the adjustability and high selectivity of the notched absorbers. At the end of this paper, an FSA-backed monopole antenna is simulated and measured, which clearly illustrates that these FSAs can serve as the ground plane for antennas and realize out-of-band RCS reduction.**

***Index Terms*—tunable notch, frequency-selective absorber (FSA), RCS reduction, equivalent circuit model (ECM)**

I. Introduction

ABSORBERS are widely used in stealth technology, RCS reduction, radomes, electromagnetic shielding, and many other applications that may reduce or selectively reduce reflection or transmission of electromagnetic waves. Research on absorbers began in 1952 when the first absorber was proposed by Salisbury [1] with a quarter-wavelength thickness, which utilizes the λ/2 path difference between the incident wave and the return wave to achieve mutual cancellation. A Salisbury absorber is characterized by its simple principle, whereas it suffers from limited bandwidth. Multilayered Salisbury screen (Jaumann absorber [2]) is one solution to improve bandwidth; however, stacked layers end with a large thickness. The wedge-tapered absorber [3] proposed in 1971 showed the best absorption while also having a cumbersome structure.

Circuit analog absorber [4], which was proposed around the turn of this century, achieved a wider frequency response while maintaining a lightweight. Instead of homogeneous resistive sheets, band-stop FSSs were applied to absorbers, which were modeled by series RLC components. FSSs can be divided into conductive FSSs (lossless FSSs) and resistive FSSs (lossy FSSs). When applied to absorbers, lossy FSSs are either made using resistive sheets [5] or loading lumped resistors [6]. Employing multiple resonances, single-layer wideband absorbers were implemented with a rather thin structure. Recently, there have also been some novel absorber designs, such as adopting the combination of plasma and resistive FSS [7], fractal FSS [8], and absorbers on the base of a magnetic substrate and FSS [9]. As we can see, however, no matter how innovative the designs, they are most often combined with FSSs.

At present, the demand for absorbers mainly lies in slimmer and lighter structures, broader bands, and better absorption effects. At the same time, for different application scenarios, such as radomes, in addition to the absorption performance, there are also needs for allowing electromagnetic waves to transmit through the radomes in the operation band without distorting the radiation performance of the antennas. These are the so-called frequency-selective absorbers (FSA) [10] that generate a transmission band [11], [12] on the basis of a wideband absorber. Additionally, notched absorbers [13], [14] that can be used as antennas' ground plane, serving as an FSS reflector, are designed to realize low-RCS antennas, which are another type of FSA, or more specifically, absorptive frequency-selective reflector (AFSR).

The design of a reflection band, either narrow or wideband, between two absorptive bands is not challenging work, if both the lossy and lossless FSSs are tuned simultaneously. However, realizing a reconfigurable and narrow reflective band with low insertion loss by merely tuning the lossless FSS is a considerable challenge.

In this paper, we first derived a theoretical formula based on transmission line theory to indicate that the notch can be flexibly tuned by only adjusting the lossless layer. The absorption and reflection mechanism of the proposed FSS

This work was supported by the National Natural Science Foundation of China (61701448 and 61671415) and the Fundamental Research Funds for the Central Universities (18CUCTJ076). *(Corresponding authors: Jianxun Su; Qingxin Guo.)*

Y. Ding, M. Li, Q. Guo, and Z. Li are with the State Key Laboratory of Media Convergence and Communication and the School of Information and Communication Engineering, Communication University of China, Beijing 100024, China (e-mail: nxdingyx@163.com, lmy_88515@sina.com, qxguo@cuc.edu.cn, zrli@cuc.edu.cn).

J. Su and H. Yin are with the School of Information and Communication Engineering, Communication University of China, Beijing 100024, China and the Science and Technology on Electromagnetic Scattering Laboratory, Beijing, 100854, China (e-mail: sujianxun_jlgx@163.com, yinhc207@126.com).

J. Song is with the Department of Electrical and Computer Engineering, Iowa State University, Ames, IA 50011, USA (e-mail: jisong@iastate.edu).

This article has been accepted for publication in a future issue of this journal, but has not been fully edited. Content may change prior to final publication. Citation information: DOI 10.1109/TAP.2020.3026889, IEEE Transactions on Antennas and Propagation

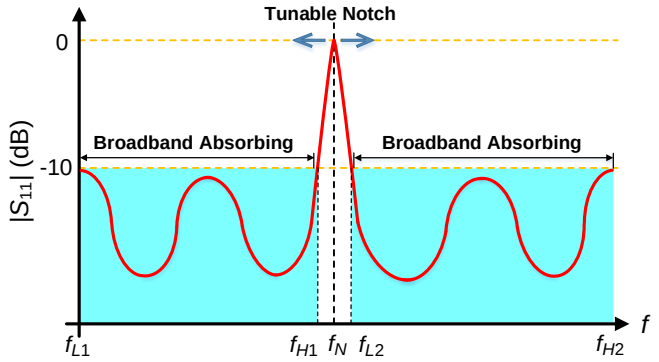

Fig. 1. Absorption and reflection mechanism of an FSA with a tunable notch.

absorbers is shown in Fig. 1. Our research showed that the absorption band (f_{L1}~f_{H2}) and the notch f_N can be controlled independently by the lossy layer and lossless layer, respectively. The independent design of the lossy layer and the lossless layer greatly simplifies the design process of the FSA with a dynamically tunable and highly selective notch. High selectivity (narrow reflection band) can guarantee two wide absorptive bands (f_{L1}~f_{H1} and f_{L2}~f_{H2}), which can ensure good stealth performance. In most previous publications, the bandwidth of two absorption bands is limited. The dynamically tunable notch can better meet wideband antenna application. Both cases for electrically and geometrically tunable notches are provided for different application scenarios.

The remainder of this paper is organized as follows. In Section II, the rationale for the independently regulated notch-band is analyzed. The modeling and performance of two absorbers with geometrically and electrically adjustable notches are detailed in Section III separately. In Section IV, taking the geometrically controlled notched absorber as an example, the numerical solution of impedance conditions for the metal-backed band-notched absorber is derived based on the general equivalent circuit model (ECM). Strict ECMs are calculated in Section V. The fabricated and measured prototypes are described in Section VI, and one application scenario of our proposed FSA serving as a monopole's ground plane is given with a time-domain simulation and actual measurement results. Section VII provides concluding remarks.

II. Derivation of the Notch-Band Control Principle

As we know, an infinite periodic structure in free space can be seen as a space filter of electromagnetic waves, which is equivalent to a two-port network [15]. The free space and substrates are equivalent to transmission lines of corresponding electrical length with characteristic impedance $Z_0 = 120\pi\ \Omega$ and $Z_1 = Z_0/\sqrt{\varepsilon_r}$, respectively. The metal-backed substrate is equivalent to short-circuited transmission lines. The general ECM for a metal-backed notched absorber is shown in Fig. 2. Each FSS layer is equivalent to a shunt impedance in the circuit,

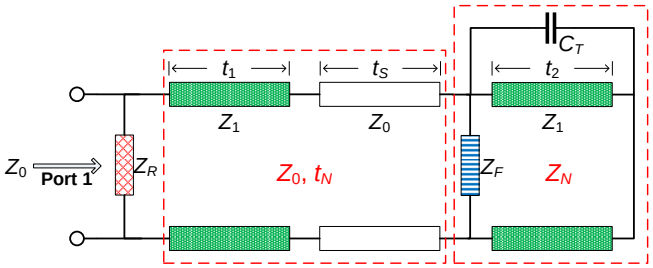

Fig. 2. General ECM for notched absorbers.

where $Z_R = R_R + jX_R$ and $Z_F = jX_F$ denote the equivalent impedance of the lossy FSS and lossless FSS, respectively. The coupling effect between the lossless FSS and the metal ground is represented by C_T.

To further analyze the reflection mechanism and the regulating principle of the notch band, we derive a simplified circuit of the notched absorber. For the sake of simplicity, the equivalent electrical length from Port 1 to the lossless FSS layer is approximately expressed as a total $t_N \approx t_1\sqrt{\varepsilon_r} + t_S$, and the lossless FSS as well as the supporting substrate and the metal ground are considered together as a reactive load of $Z_N = jX_N$ (see the red dotted boxes in Fig. 2). Therefore, the transfer matrix can be simplified as follows:

$$\begin{bmatrix} A & B \\ C & D \end{bmatrix} = \begin{bmatrix} 1 & 0 \\ \dfrac{1}{Z_R} & 1 \end{bmatrix} \begin{bmatrix} \cos\delta_N & jZ_0\sin\delta_N \\ j\dfrac{\sin\delta_N}{Z_0} & \cos\delta_N \end{bmatrix} = \begin{bmatrix} \cos\delta_N & jZ_0\sin\delta_N \\ \dfrac{\cos\delta_N}{R_R + jX_R} + \dfrac{j\sin\delta_N}{Z_0} & \cos\delta_N + \dfrac{jZ_0\sin\delta_N}{R_R + jX_R} \end{bmatrix}, \tag{1}$$

where $\delta_N = \beta t_N = (2\pi t_N/c)f$ is the total phase path between lossy FSS and lossless FSS.

The reflection coefficient at the notch frequency is calculated as follows:

$$|S_{11}| = \left|\frac{AZ_N + B - CZ_0Z_N - DZ_0}{AZ_N + B + CZ_0Z_N + DZ_0}\right| = 1. \tag{2}$$

It should be mentioned that the absorption rate is calculated as $1 - |S_{11}|^2$ with $S_{21} = 0$ for the metal-backed absorbers throughout the whole discussion.

The complete expression of (2) is shown at the bottom of this page. The analytical solution to X_N is

$$X_N = -Z_0\tan\delta_N. \tag{3}$$

Thus, the notch frequency f_N can be expressed by

$$f_N = \frac{c}{2\pi t_N}\arctan\left(-\frac{X_N}{Z_0}\right). \tag{4}$$

That is, when the thickness of dielectric slabs is fixed, the notch frequency has a function relationship with the reactance X_N of the lossless layer and is independent of the lossy layer. We thereby prove that the notch frequency can be fully

$$|S_{11}|^2 = \frac{\left(jX_N + Z_0 - X_N\tan\delta_N + jZ_0\tan\delta_N - \dfrac{jZ_0^{\,2}\tan\delta_N}{R_R - jX_R} - \dfrac{jX_NZ_0}{R_R - jX_R}\right)\left(jX_N - Z_0 + X_N\tan\delta_N + jZ_0\tan\delta_N - \dfrac{jZ_0^{\,2}\tan\delta_N}{R_R + jX_R} - \dfrac{jX_NZ_0}{R_R + jX_R}\right)}{\left(jX_N + Z_0 - X_N\tan\delta_N + jZ_0\tan\delta_N + \dfrac{jZ_0^{\,2}\tan\delta_N}{R_R - jX_R} + \dfrac{jX_NZ_0}{R_R - jX_R}\right)\left(jX_N - Z_0 + X_N\tan\delta_N + jZ_0\tan\delta_N + \dfrac{jZ_0^{\,2}\tan\delta_N}{R_R + jX_R} + \dfrac{jX_NZ_0}{R_R + jX_R}\right)} = 1$$

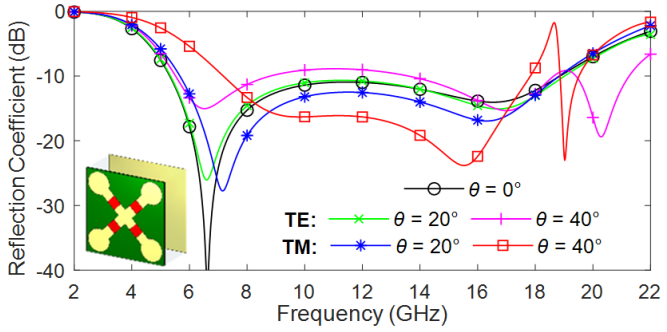

Fig. 3. Reflection coefficient of a crossed dipole-shaped wideband absorber under different incident angles.

controlled by adjusting the lossless layer while the absorption band remains stable. The independent design of the lossy layer and the lossless layer greatly simplifies the design process of an FSA with a dynamically tunable and highly selective notch.

III. Modeling and Performance of Two Absorbers

A. FSA with a Geometrically Controlled Notch-Band

For the first absorber designed with a geometrically controlled notch-band, a crossed dipole-shaped wideband absorber loaded with four lumped resistors is used as a baseline, which is composed of two perpendicular dipole-shaped [16], [17] patches in each unit and has a period of 10.2 mm. More than 10 dB RCS reduction for two polarizations is realized with a ratio bandwidth over 3.55 within the incident angle of 40º.

The lumped resistors are used to realize wideband impedance matching between the structured absorber and free space. The absorption performance is mainly attributed to the lumped resistors due to the low dielectric loss. The absorption characteristic of the proposed wideband absorber (without a notch) is simulated and analyzed by the frequency domain solver of CST, as shown in Fig. 3.

To generate a notch within the absorption band, a lossless FSS and a substrate supporting it are added to the wideband absorber. The complete model of the notched absorber is shown in Fig. 4. A deformation exists at the end of dipoles to increase terminal capacitance. The sensitivity to incident angles and polarization has been decreased due to its rotationally symmetric and compact structure.

It is well-known that the free space wave impedance at oblique incidence varies with polarization, and the reflection coefficient varies accordingly. Any polarization can be decomposed into TE and TM waves, while $Z_0^{TE} = Z_0/\cos\theta$ and $Z_0^{TM} = Z_0\cos\theta$. The impedance variation trends with incident angle are opposite for the two polarizations, which means it is impossible to achieve perfect impedance matching for two polarizations simultaneously under oblique incidences; there must be compromises between these two polarizations. As shown in Fig. 5, the absorption bands are well-maintained when the incident angle is less than 40° for TE polarization or is less than 30° for TM polarization. With an increasing incident angle, the lowest frequency of the grating lobes decreases [4], i.e., more grating lobes appear in the operating frequency band, leading to deterioration of angular stability. In addition to the grating lobes, for TM only, we can see spikes at

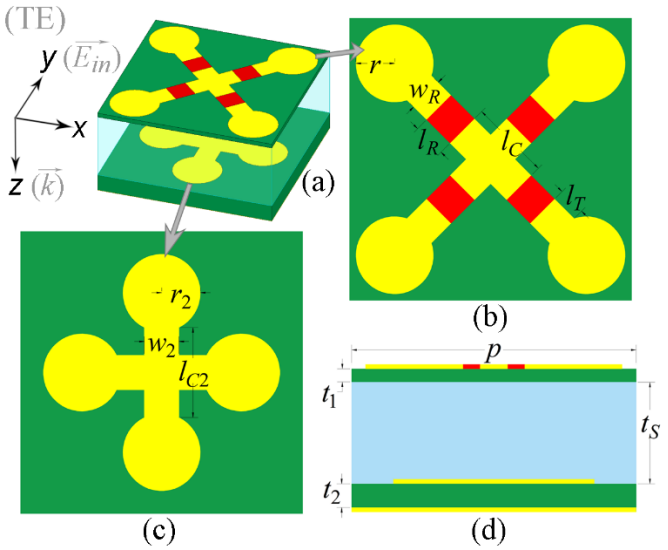

Fig. 4. Unit cell of the first absorber with a geometrically controlled notch band. The four chip resistors with a resistance value R = 125 Ω are indicated in red. (a) Perspective view. (b) Upper lossy layer. (c) Lower lossless layer. (d) Side view. (l_R = 1.2 mm, w_R = 1.25 mm, r = 1.4 mm, l_C = 2.9 mm, l_T = 1 mm, t_1 = 0.25 mm, t_S = 3.8 mm, t_2 = 1 mm, r_2 = 1.4 mm, w_2 = 1.25 mm, l_{C2} = 3.25 mm and p = 10.2 mm)

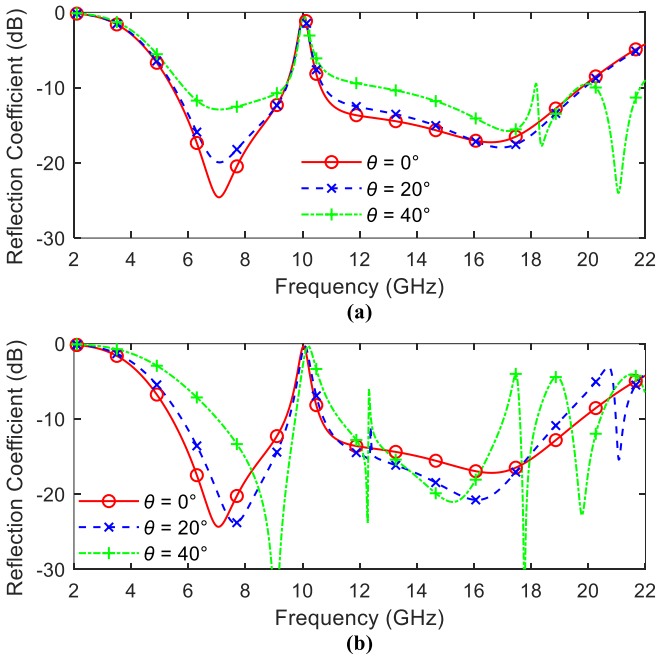

Fig. 5. Reflection coefficient of a geometrically controlled notched absorber under different incident angles. (a) TE polarization. (b) TM polarization.

12.35 GHz under oblique incidences, which are the so-called Fano resonance [18]. These polarization-dependent Fano peaks result from the asymmetry of the lossless layer at oblique incidences. As we know, for TE polarization, the incident electric field is always in the y-direction. But for TM polarization, when the FSS is incident with an angle θ, there is a pitch angle between the incident electric field and the FSS plane, thus the symmetry of the system is destroyed, and as a result, Fano resonance is enhanced.

One advantage of our design is that the position of the sharp notch is completely controlled by the lossless FSS whose shape

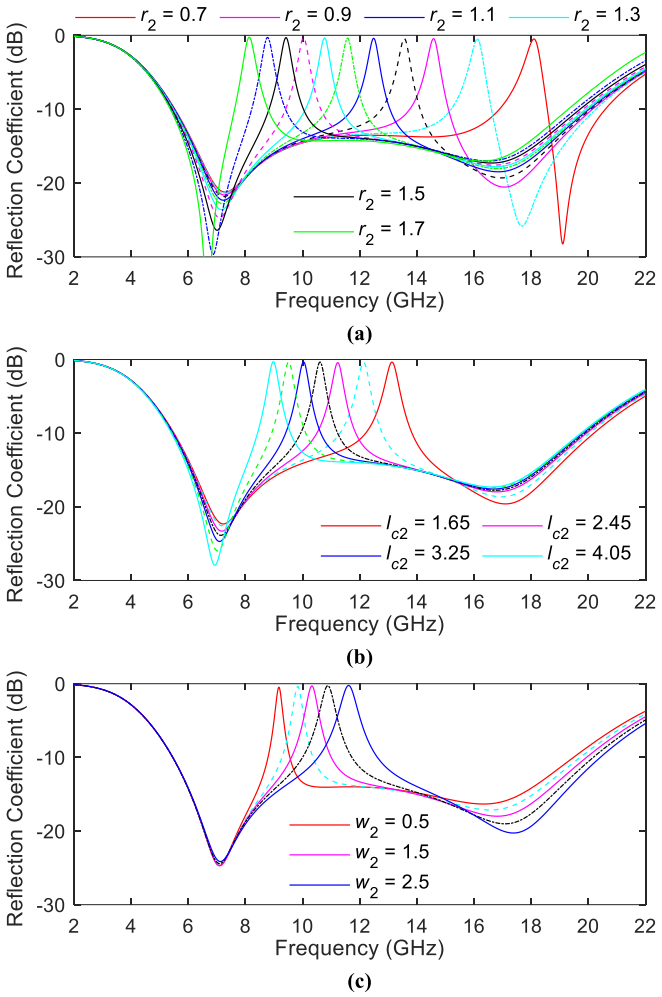

Fig. 6. Reflection coefficient of the geometrically controlled notched absorber with different length values of (a) r_2, (b) l_{C2}, and (c) w_2 (mm).

is determined by three parameters. By adjusting these three parameters, the center frequency of the notch-band can be adjusted across the whole band. The frequency-domain simulation results are shown in Fig. 6.

In fact, with the other two parameters fixed, simply changing r_2 can adjust the notch position throughout the entire frequency band, as shown in Fig. 6(a). As r_2 increases, the center of the notch moves to the lower frequencies.

With r_2 and w_2 fixed, changing l_{C2} can adjust the notch position over a relatively narrow band, as shown in Fig. 6(b). As l_2 increases, the center of the notch moves to lower frequencies. When l_2 increases from 0.4 to 0.5 mm, there is a hop in the position of the notch and a loss in bandwidth; therefore, the value of l_2 should not be too large.

With r_2 and l_2 fixed, changing w_2 can fine-tune the notch position, which is shown in Fig. 6(c). As w_2 increases, the center of the notch moves to higher frequencies. Meanwhile, w_2 affects the width of the notch-band. As w_2 increases, the notch becomes wider, resulting in poor selectivity; therefore, the value of w_2 should not be too large.

B. FSA with an Electrically Controlled Notch-Band

The second notched absorber has a similar structure to the first but has different FSS patterns. This absorber is designed

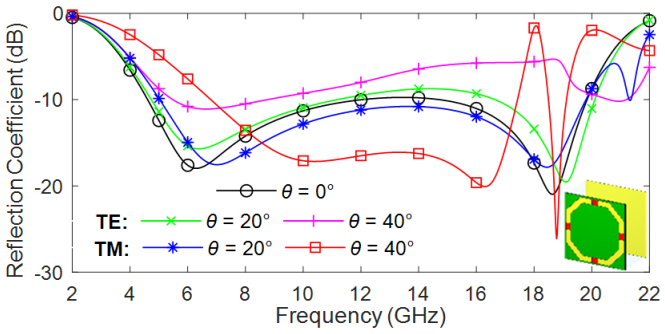

Fig. 7. Reflection coefficient of an octagonal ring-shaped wideband absorber under different incident angles.

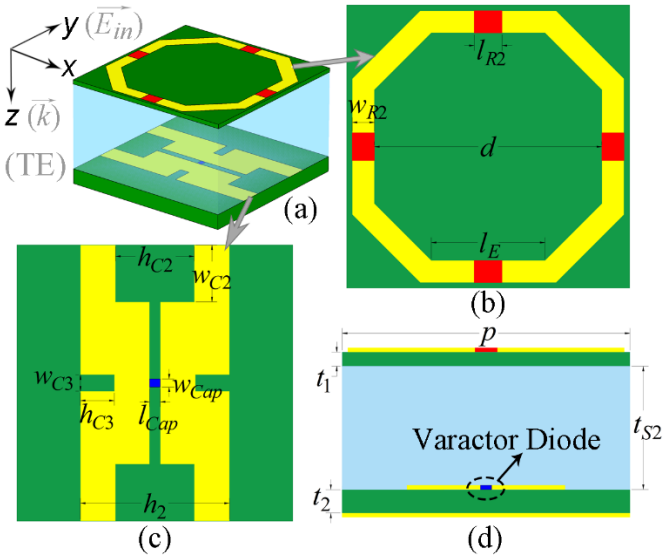

Fig. 8. Unit cell of the second absorber with an electrically controlled notch band. The four chip resistors with a resistance value R_2 = 340 Ω are indicated in red. (a) Perspective view. (b) Upper lossy layer. (c) Lower lossless layer. (d) Side view. (l_{R2} = 1 mm, w_{R2} = 0.8 mm, l_E = 4.1 mm, d = 8.2 mm, t_1 = 0.5 mm, t_{S2} = 4.4 mm, t_2 = 1 mm, l_{Cap} = 0.4 mm, w_{Cap} = 0.3 mm, h_2 = 5.5 mm, h_{C2} = 2.9 mm, w_{C2} = 2.1 mm, h_{C3} = 1.3 mm, w_{C3} = 0.6 mm, and p = 10.2 mm)

based on an octagonal ring-shaped wideband absorber (see inset in Fig. 7). The lossy FSS of this absorber is composed of an octagonal ring and four lumped resistors in each unit and is rotationally symmetric. Good absorption performance is achieved within the incident angle of 30° for both TE and TM polarizations, as displayed in Fig. 7. The operating frequency band ranges from 4.63 GHz to 19.82 GHz for normal incidence.

Fig. 8 shows the unit cell structure of the second notched absorber. A major difference from the geometrically controlled absorber is the use of a varactor diode on its lossless layer, which makes it possible to shift the notch position electrically. Hence, one can implement a real-time adjustment of the notch-band by simply changing the bias voltage of the varactor. The lossless layer is based on an H-shaped pattern with a narrow slot on the edge, which permits a *y*-polarized notch, as seen in Fig. 9(a). When the incident electric field is perpendicular to the direction of the varactor diode, which means the varactor diode is inactive and the induced current on the lossless layer is very low; therefore, there will be no notch-band. The H-shaped structure also makes it easy to apply a bias voltage to the varactor diodes. To narrow the notch-band and achieve high

This article has been accepted for publication in a future issue of this journal, but has not been fully edited. Content may change prior to final publication. Citation information: DOI 10.1109/TAP.2020.3026889, IEEE Transactions on Antennas and Propagation

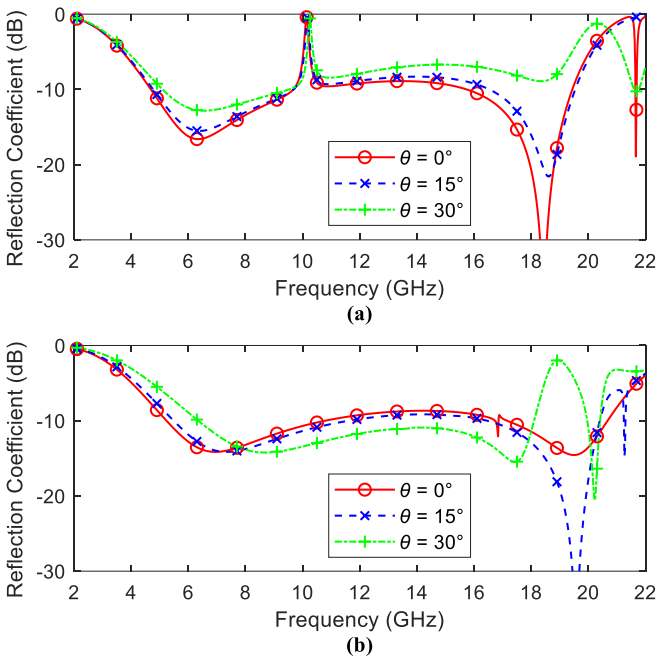

Fig. 9. Reflection coefficient of an electrically-controlled notched absorber under different incident angles when the capacitance value C of the varactor diode is 0.4 pF. (a) TE polarization. (b) TM polarization.

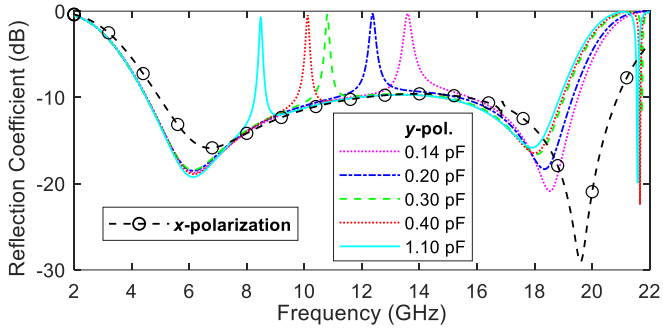

Fig. 10. Reflection coefficient of the electrically controlled notched absorber with different capacitance values C (pF).

selectivity, some deformation is adopted with no more tautology. The simulation results of oblique incidences are shown in Fig. 9.

The type of varactor diode we chose is a MA46H120 with low parasitic capacitance and high Q, and the varactor has a linear tuning range from 0.14 pF to 1.1 pF. As shown in Fig. 10, the notch frequency decreases with increasing capacitance C under y-polarization. For x-polarization, the absorber retains wideband absorption characteristics and will not be affected by the capacitance C of the varactor. Therefore, when applied to antennas, the antenna polarization should be consistent with the polarization of the notch, which can effectively ensure antenna gain and achieve good stealth performance for both polarizations.

IV. Impedance Condition for Notched Absorbers

In this part, all numerical calculations are based on the geometrically controlled notched absorber. The electrically controlled design can be solved similarly. To simplify the calculation of the numerical solution, only the impedance values of FSSs are set as dependent variables.

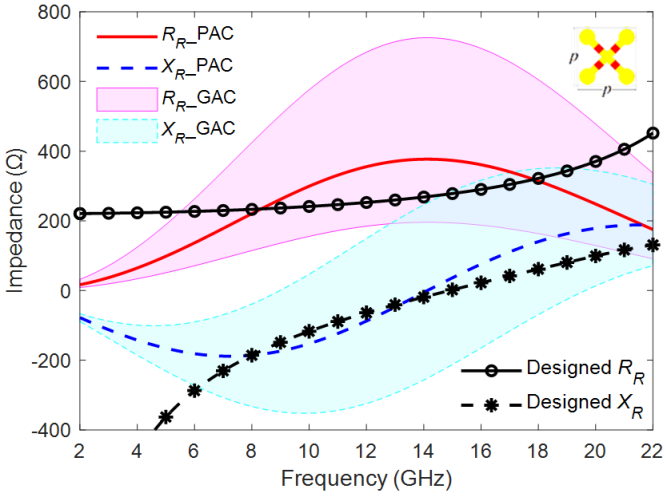

Fig. 11. Perfect absorption condition (PAC) curves and general absorption condition (GAC) value range of lossy FSS for wideband absorber compared with impedance values of the freestanding lossy FSS in our design (t_1 = 0.25 mm and t_S = 4.9 mm).

First, we plug in the thickness values of the wideband absorber and calculate the values of Z_R that meet the absorption conditions. The equation $|S_{11}| = 0$ is solved numerically at each frequency point with the help of MATLAB, enabling us to obtain R_R and X_R curves satisfying the perfect absorption condition (PAC). For a practical design, we usually choose $|S_{11}| < -10$ dB (with a linear value of 0.316) as a criterion to evaluate the absorption performance, which was referred to as a general absorption condition (GAC) [15]. We successively get the value ranges of R_R and X_R satisfying GAC when X_R and R_R are constrained to PAC respectively. When both the real part and the imaginary part of Z_R come within the areas defined by GAC, less than −10 dB reflection can be realized. As shown in Fig. 11, the impedance values of the freestanding lossy FSS in our design lie in the absorption areas at the operating band.

Then comes the generation of the notch-band. From this point forward, we take into account Z_F, C_T, and t_2. As before, the thickness t_2 is set to a constant.

It should be noted that the coupling capacitance C_T is considerable when calculating the notch frequency f_N, which can be confirmed by observing the distribution of the electric field. The value of C_T directly depends on the dimensions of the lossless FSS, and because the dimensions of lossless FSS determine the notch frequency f_N, we can deduce that C_T has a function relationship with f_N. Using simulation software Ansys Electronics Desktop, we can get impedance curves of the freestanding lossless FSS and the lossless FSS backed with a grounded substrate, namely Z_F and Z_N (see Fig. 2), respectively. With the help of the optimization tool of ADS, we determined the values of C_T for different length values of r_2, then the relationship between C_T and f_N is obtained by curve fitting.

$$C_T = \frac{1}{0.0421 f_N^{\,2} - 0.2142 f_N + 1.0366} \tag{5}$$

Plugging in the designed Z_R of the upper lossy FSS, the reflection condition is calculated in an ideal world with $|S_{11}| = 1$ and in a practical situation with less than 0.5 dB insertion loss,

This article has been accepted for publication in a future issue of this journal, but has not been fully edited. Content may change prior to final publication. Citation information: DOI 10.1109/TAP.2020.3026889, IEEE Transactions on Antennas and Propagation

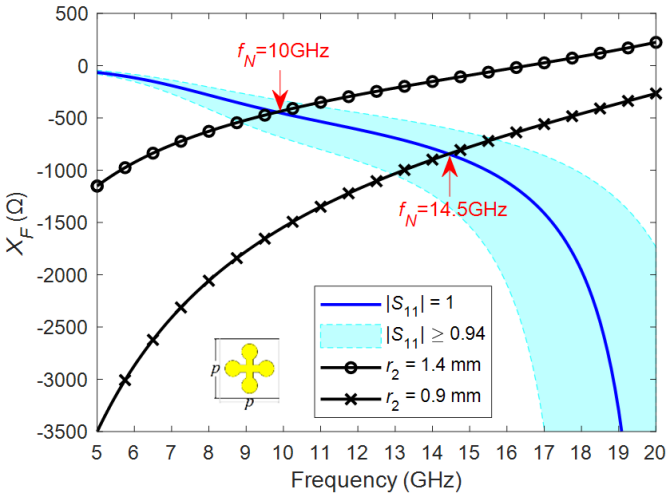

Fig. 12. Impedance conditions of freestanding lossless FSS at notch frequencies compared with impedance values of our designed lossless FSSs. (t_1 = 0.25 mm, t_S = 3.8 mm and t_2 = 1 mm)

i.e., $|S_{11}| \geq -0.5$ dB (linear value of 0.94). The result is shown in Fig. 12. Through comparison with the designed impedance values of the freestanding lossless FSS, the notch frequency can be recognized and corresponds to the simulation results of Ansys Electronics Desktop. Moreover, the light blue ($|S_{11}| \geq 0.94$) can be seen to widen, which means the selectivity of notch-band worsens as f_N increases, and this trend is consistent with full-wave simulation result (see Fig. 6). The slight discrepancies should be attributed to the coupling effect between lossy FSS and lossless FSS, which is relatively weak and is not taken into consideration in the general ECM.

V. Equivalent Circuit Extraction and Analysis

By observing the distribution of electric field and magnetic field, the distribution of equivalent capacitance and inductance can be roughly inferred (see Fig. 14). For the geometrically controlled notched absorber, we see that the magnetic field concentrates on the metal cross in the center. The coupling between units is primarily electric coupling, which exists between the ends of adjacent dipoles, and the coupling is stronger at lower frequencies. As frequency increases, the coupling between units weakens, and the electric coupling is gradually distributed between the intersecting dipole ends within a unit. In general, we can deduce that the equivalent capacitance generated by the interaction between units is larger than that from within a unit, i.e., C_{11} representing the equivalent capacitance between units is much larger than C_{12} representing the terminal capacitance within a unit. The metal cross in the center contributes to the equivalent inductance L_1.

Similarly, for the octagonal ring-shaped lossy FSS of the electrically controlled notched absorber, it can be seen from the electric field distribution that the electric coupling between units is stronger at lower frequencies, and mainly spreads over the gaps in the direction of the incident electric field. Meanwhile, the magnetic field concentrates on the metallic stripes along the incident electric field. Two arms perpendicular to the incident electric field have almost no current flowing through. The equivalent capacitance in the direction of the incident electric field is much larger, that is, C_{31}

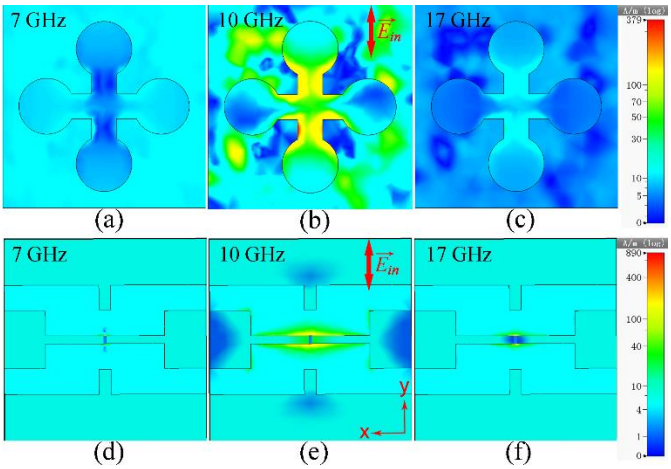

Fig. 13. Surface current distribution of lossless FSS layers at a lower absorption band of 7 GHz, notch frequency of 10 GHz, and higher absorption band of 17 GHz. (a)-(c) Geometrically controlled lossless layer. (r_2 = 1.4 mm) (d)-(f) Electrically controlled lossless layer under *y*-polarization. (C = 0.4 pF)

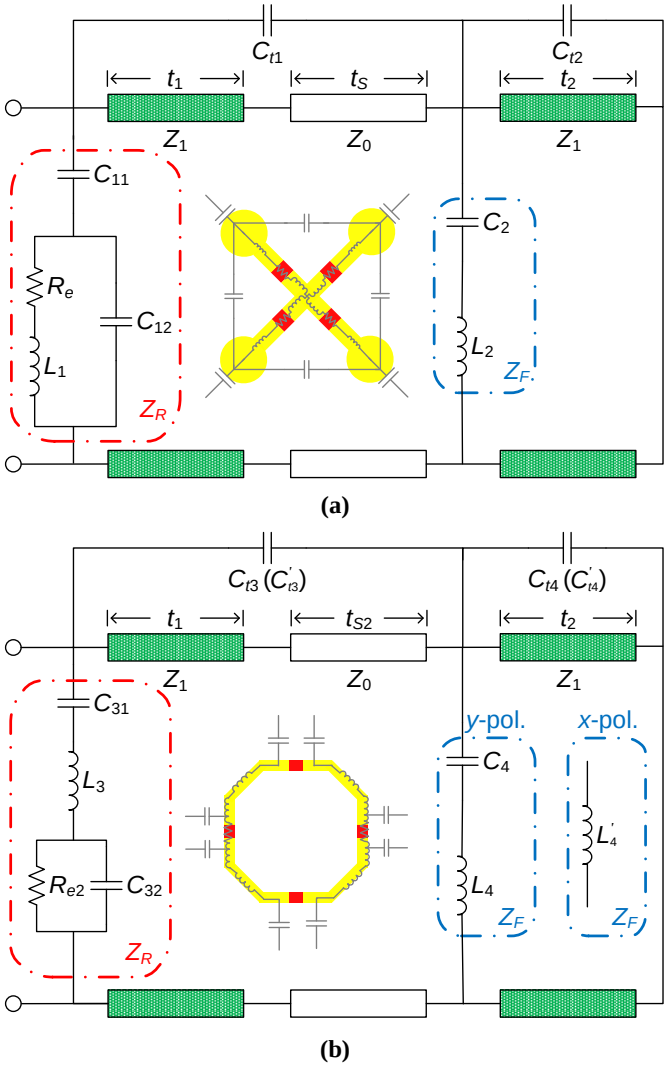

Fig. 14. Integrated ECM for (a) geometrically controlled notched absorber of two polarizations and (b) electrically controlled notched absorber of *y*- and *x*-polarization, respectively.

is much larger than C_{32}. In this context, the octagonal rings loaded with resistors are modeled as distributed RLC components.

The band-stop FSS in free space, which can be modeled by a series LC circuit, resonates to be zero impedance when it presents reflection characteristics, and it is inductive below the resonant frequency and capacitive above the resonant frequency. In addition to the rigorous calculations in Section IV, there is a simple method to estimate the resonance frequency of the band-stop lossless FSS in the geometrically controlled FSA.

The traditional cross-shaped FSS is composed of two orthogonal microstrip lines, which allow it to work with an electric field in either direction. In free space, the first resonance occurs at a frequency point where the length of the microstrip line equals half-wavelength [19]. In this instance, the lossless FSS is almost sandwiched by two F4B substrates, which makes the resonance frequency of the freestanding lossless FSS go down by about $\sqrt{\varepsilon_r}$ [4], [20]; that is, the resonance frequency of the lossless FSS can be roughly estimated as $c/(2l_e \times \sqrt{\varepsilon_r})$, where l_e is the length of the microstrip line. However, while employing a traditional cross-shaped FSS to produce a notch, the adjustable range of notch-band is limited with a large insertion loss. To overcome these shortcomings, the crosswise dipole-shaped FSS with $l_e \approx l_{C2} + 4r_2$ is designed to increase terminal capacitance, and as a result, a sharp notch with an insertion loss less than 0.5 dB is obtained, which can be adjusted across the whole band.

To further validate the circuit model, the surface current distribution of the lower band-stop FSS is shown in Fig. 13. Strong surface current is excited only at the notch frequency, and mainly along the direction of the incident electric field. At other frequencies, very low surface current is induced on the surface of the lossless FSS, which means that the tangential electric field is very weak, and consequently, the band-stop FSS is transparent to EM waves and the FSA works as a wideband absorber.

The lossless FSS of the electrically controlled absorber, which is loaded with a varactor, is designed with several gaps to increase the distributed capacitance. After the simulation, it can be seen that the electric field concentrates on the meandering edges of the shape. Strong surface current is induced around the varactor at notch frequency, and a notch-band can only be generated under a *y*-polarized wave (see Fig. 13(e)) when the incident electric field is parallel to the varactor. For *x*-polarization, because the incident electric field is perpendicular to the varactor, very low surface current is induced on the lossless layer, and as a result, there will be no notch-band. Moreover, changing C cannot influence Z_F; thus, the S_{11} curve is not affected by the varactor and remains unchanged under *x*-polarization.

A general ECM for metal-backed notched absorbers has been discussed in Section II, as is shown in Fig. 2, where variables are functions of both frequency and dimension. For the variables in ECM to be independent of frequency, the upper lossy FSS is modeled by an RLC network [15], and the lower band-stop FSS is modeled by a series LC circuit. To accurately model the absorber under specific dimensions and values, C_{t1} is introduced to ECM, which represents the coupling effect between lossy FSS and lossless FSS and is much smaller than C_{t2}. The final circuit schematics of our proposed FSAs are presented in Fig. 14. The first FSA is rotationally symmetric, so its ECM is the same for two polarizations under normal incidence.

TABLE I
OPTIMIZED VALUES OF ECM COMPONENTS FOR TWO FSAS

C_{11}/pF	C_{12}/pF	L_1/nH	R_e/Ω	C_2/pF
0.08	0.01	1.86	211.42	0.03
L_2/nH	C_{t1}/pF	C_{t2}/pF	C_{31}/pF	C_{32}/pF
1.92	0.01	0.3	0.13	0.03
L_3/nH	R_{e2}/Ω	C_4/pF	L_4/nH	C_{t3}/pF
3	269.74	0.04	1.49	0.03
C_{t4}/pF	L'_4/nH	C'_{t3}/pF	C'_{t4}/pF	
0.2	0.5	0.03	0.25	

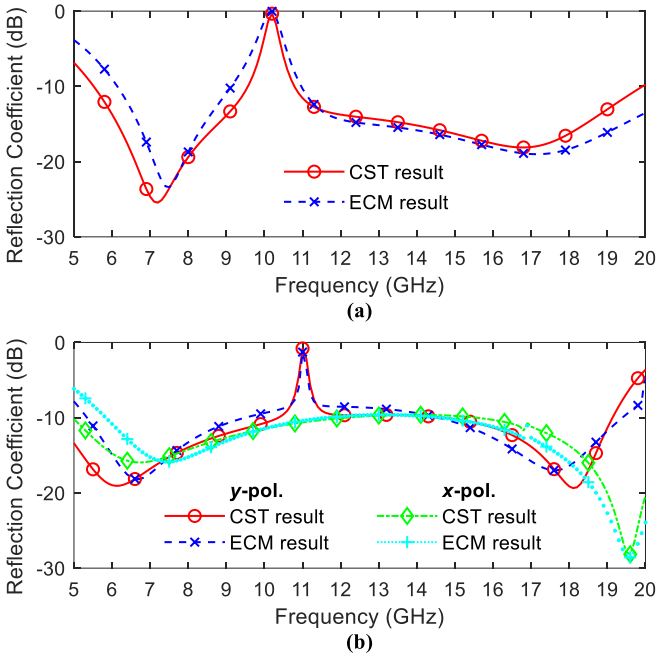

Fig. 15. Reflection coefficients obtained via full-wave simulation and equivalent circuit calculation. (a) Geometrically controlled notched absorber with r_2 = 1.4 mm. (b) Electrically controlled notched absorber with C = 0.4 pF.

As shown in Fig. 14(a), chip resistors in each unit are in parallel, so we have modified the formula in [21] and the total equivalent resistance can be estimated as

$$R_e \approx \frac{R_S}{N}\frac{S}{S_R}, \tag{6}$$

where S is the patch area corresponding to the resistance branch, S_R is the surface area of a chip resistor, $R_S = R \times w_R/l_R$ is the surface resistance of chip resistors and N is the number of branches in parallel.

The above estimated R_e from observations is not accurate, so the optimization tool of Ansys Electronics Desktop is used to approximate the S_{11} results of the full-wave simulation when impedance values of the freestanding FSSs have been taken as a reference primarily. The optimized parametric values of equivalent circuits are listed in Table I. The S_{11} result of our proposed ECM is consistent with the S_{11} curve simulated by CST (see Fig. 15). In the ECM, the dielectric loss is not taken

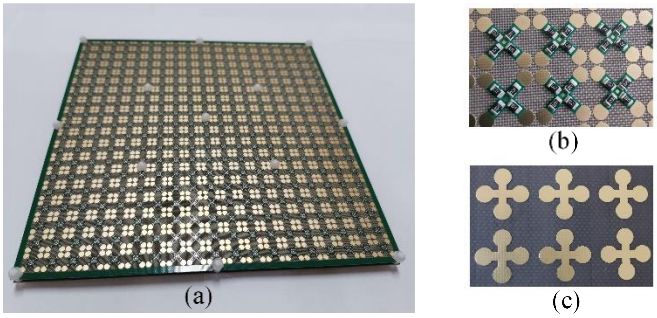

Fig. 16. Photos of the fabricated geometrically controlled FSA. (a) Assembled absorber. (b) Upper lossy layer. (c) Lower lossless layer.

into account, and only major distributed components are introduced, which are the main causes of deviation from the simulation results.

VI. Experimental Verification

In this section, samples of the proposed FSAs with geometrically controlled and electrically controlled notch-band have been manufactured and tested.

A. Measurement of a Geometrically Controlled FSA

For the geometrically controlled FSA, which is composed of 19 × 19 unit cells and is 200 × 200 mm^2 in size, we fabricated one lossy layer and one lossless layer and assembled them successively with nylon screws. As explained before, for the geometrically controlled FSA, we can obtain different notch frequencies by replacing lossless layers of different dimensions. In this experiment, we choose two instances with the only difference of r_2, which has a length of 1.4 mm and 0.9 mm respectively, and their time-domain simulation results from CST are provided to validate the adjustability of the notch-band.

As shown in Fig. 16, the metallic patterns were printed on F4B substrates using printed circuit board (PCB) technology, and four chip resistors (0805, 120 Ω) were soldered on the copper strips of each resistive element using surface mount technology. In case of warping of the upper thin substrate, thirteen isolated columns have been sandwiched between the upper substrate and the lower substrate to keep them parallel.

The absorbing/reflecting performance of the geometrically controlled FSA was measured by the compact antenna test range system at the Science and Technology on Electromagnetic Scattering Laboratory in Beijing, China [22], [23]. To improve measurement precision, five pairs of standard linearly polarized horn antennas working at 4-6 GHz, 6-8 GHz, 8-12 GHz, 12-18 GHz, and 18-24 GHz were used for transmitting and receiving electromagnetic waves. The RCS is measured using a Keysight N5234A vector network analyzer. To eliminate the interferences from multiple reflections and the coupling effect between two horns, the time-domain gating function of the network analyzer was used to accurately measure the reflected wave. The RCS reduction results of the prototype were obtained after calibrating with a metal ground plane test.

Fig. 17 shows a comparison of the measured and simulated RCS reduction results of the geometrically controlled FSA with r_2 = 1.4 mm. The measured data are largely in keeping with the

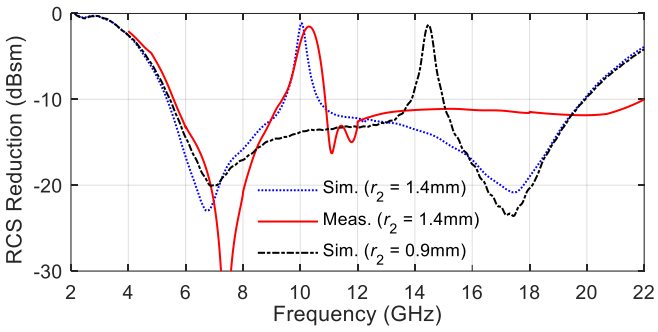

Fig. 17. Measured and time-domain simulated RCS reduction of the geometrically controlled FSA with different length values of r_2.

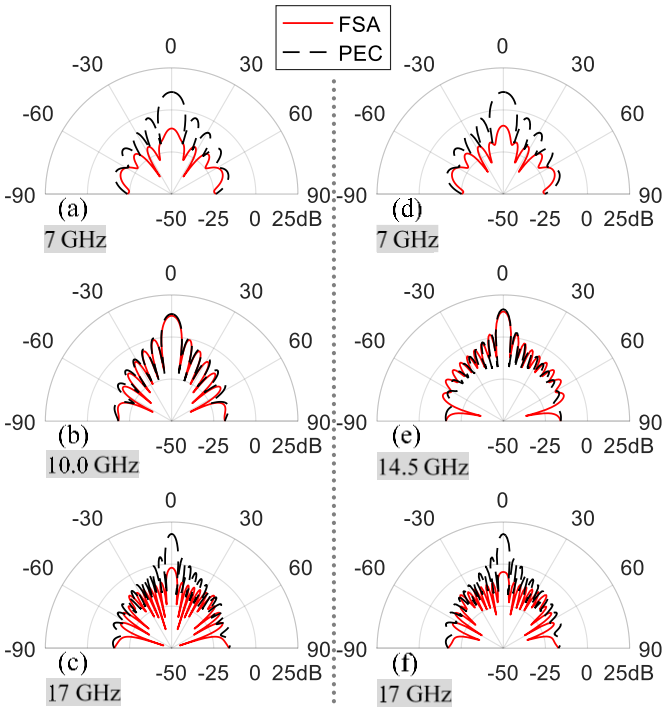

Fig. 18. Comparison of the bistatic scattering RCS between the proposed geometrically controlled FSA and equal-sized PEC surface under normal incidence at a lower absorption band of 7 GHz, notch frequencies of 10.0 and 14.5 GHz, and higher absorption band of 17 GHz, respectively. (a)-(c) Geometrically controlled FSA with r_2 = 1.4 mm. (d)-(f) Geometrically controlled FSA with r_2 = 0.9 mm.

time-domain simulation results. Except for the fabrication error and resistor value tolerances, the slight discrepancy between time-domain simulation and measurement results should be attributed to the unevenness of the handmade air layer and the parasitic effect of lumped resistors, which was not taken into account in the full-wave simulation. Compared with the frequency-domain simulation results for infinite periodic structures, the higher insertion losses result from the edge effects of finite arrays. The time-domain simulation result of r_2 = 0.9 mm is also provided. Compared with the result for r_2 = 1.4 mm, the notch frequency shifts from 10.0 GHz to 14.5 GHz. The adjustability of the notch is proven in this way.

To reflect the applicability of the geometrically controlled FSA with bistatic scenarios, the time-domain simulation results of bistatic scattering RCS in the E-plane are shown in Fig. 18.

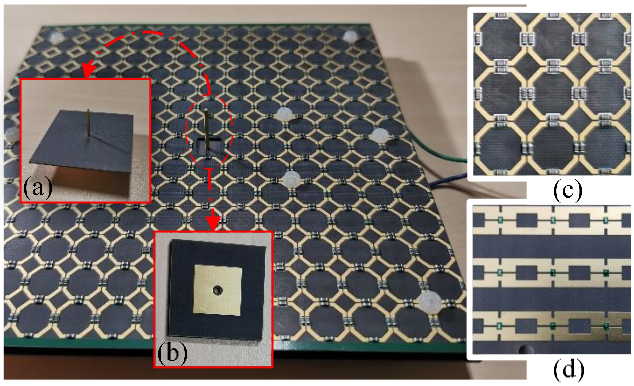

Fig. 19. Photos of the electrically controlled FSA and an FSA-backed monopole. (a) Photo of the fabricated monopole antenna. (b) Ground plane of the monopole. (c) Top lossy layer of the FSA. (d) Lower lossless layer of the FSA.

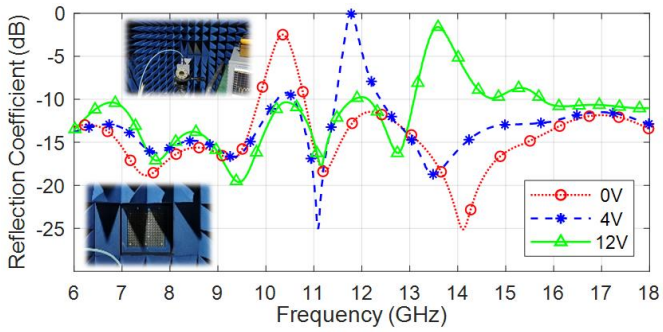

Fig. 20. Measured reflection of the electrically controlled FSA with different bias voltages.

At the absorption frequencies of 7 GHz and 17 GHz, the bistatic RCS of the FSA in the entire space is much lower than that of the equal-sized PEC ground surface. The bistatic stealth performance is better than diffuse scattering based on the phase cancellation method, whose sidelobe level will increase according to the law of conservation of energy [24]-[26]. Moreover, the FSA serves as a PEC surface where almost all incident energy is reflected at notch frequencies of 10 GHz and 14.5 GHz for r_2 = 1.4 mm and r_2 = 0.9 mm, respectively.

B. Measurement of an Electrically Controlled FSA

For the electrically controlled FSA, we fabricated a prototype with 14 × 14 unit cells, which is shown in Fig. 19. The upper lossy layer is mounted with four chip resistors (0603, 340 Ω) in each unit, and the lower lossless layer is welded with one varactor diode (MA46H120) in each unit. The size of the F4B substrates is 147 mm × 143 mm due to the addition of bias lines printed on two sides to feed the varactor diodes. For subsequent antenna-loaded tests, one unit cell has been removed. The upper lossy layer is held up with 10 nylon screws and gaskets to keep a 4.4 mm distance from the lower lossless layer.

The measurement setup is shown in the insets of Fig. 20. The electrically-controlled FSA was measured in an anechoic chamber using Keysight E5071A with time-domain gating, which was used to reduce multipath interferences during the measurement of the reflection coefficient. The aperture of the horn antenna for testing is 75 mm × 75 mm, and the horn antenna is 1 m away from the FSA. The FSA was surrounded

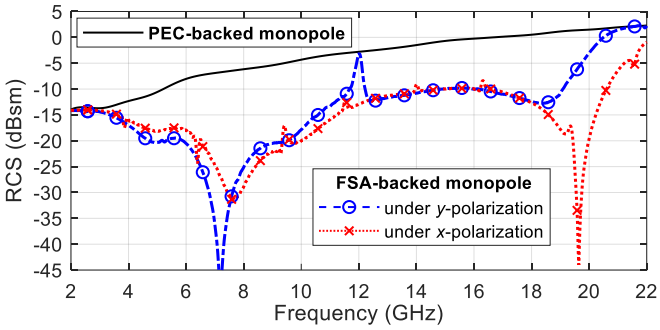

Fig. 21. Simulated RCS of an FSA-backed monopole under *y*-polarized and *x*-polarized normal incidences compared with a PEC-backed monopole.

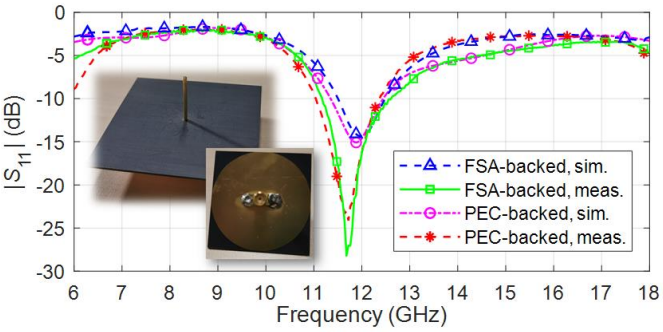

Fig. 22. Simulated and measured reflection of an FSA-backed monopole compared with a PEC-backed monopole. The insets are photos of the PEC-backed monopole.

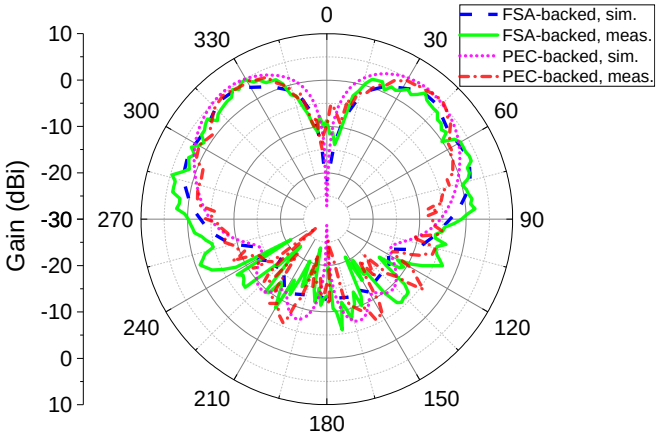

Fig. 23. Gain of an FSA-backed monopole compared with a PEC-backed monopole at notch frequency of 11.8 GHz.

with absorbent foam to reduce the effect of edge diffraction. Limited by this measurement setup, the far-field conditions were hard to meet for the entire frequency range.

In testing of the electrically controlled FSA, the notch frequency is regulated by changing the bias voltage of the varactor diodes. With an increasing bias voltage, the capacitance of the varactors decreases, thereby the notch moves to higher frequencies. As shown in Fig. 20, the variation trend of the notch-band is consistent with previous conclusions.

To illustrate the application scenario of these band-notched FSAs, we conducted experiments of a monopole antenna backed with the electrically controlled FSA. As shown in Fig. 19, we fabricated a monopole antenna, and then made the

TABLE II
PERFORMANCE COMPARISON OF BAND-NOTCHED FSAS

Ref.	Notch Band			Absorption Band		Other Attributes		
	Notch Adjustability	Tunable Range (GHz)	Insertion Loss and f_N	Absorptive Bands (GHz)	Relative Absorption Bandwidth [a]	Polarization	Cell Size (mm)	Total Thickness (mm)
[16]	No	8.2-9.8	-0.2 dB @7.9 GHz	4.8-8 & 10.2-16	86.5%	Single	16 (0.26λ_{L1}) × 11.4 (0.18λ_{L1})	6.5 (0.1λ_{L1})
[28]	No	4.15-4.56	-0.12 dB @3.54 GHz	2.05-4.02 & 4.78-7.24	95.4%	Dual	25 (0.17λ_{L1}) × 25 (0.17λ_{L1})	13 (0.09λ_{L1})
Our work (r_2 = 1.4 mm)	Yes (Geometrical)	5.35-19.9	-0.45 dB @10 GHz	5.35-9.46 & 10.63-19.9	106%	Dual	10.2 (0.18λ_{L1}) × 10.2 (0.18λ_{L1})	5.05 (0.09λ_{L1})
Our work (C = 0.4 pF)	Yes (Electrical)	8-14	-0.4 dB @10.14 GHz	4.77-10.86 & 11.96-19.08	110.8%	Single	10.2 (0.16λ_{L1}) × 10.2 (0.16λ_{L1})	5.9 (0.09λ_{L1})

λ_{L1} = free space wavelength at the lowest operating frequency f_{L1} (see Fig. 1)
[a] Relative Absorption Bandwidth: The ratio of the absorption bandwidth relative to the center frequency, which is calculated as (see Fig. 1) $2(f_{H1} - f_{L1} + f_{H2} - f_{L2})/(f_{L1} + f_{H2})$.

monopole perpendicular to the surface of the FSA. The length of the monopole is 18 mm. The monopole is fixed to an F4B substrate, which is 20 mm × 20 mm in size. A metal ground patch with a side length of 10 mm is printed on the back, as shown in Fig. 19(b).

It is learned that a well-structured FSA with more unit cells produces a better ground plane for the antenna, but there is a trade-off between efficiency and RCS. FSA-backed antennas suffer from low-efficiency, which is a compromise to low-RCS. From Fig. 21, we can see that modification to the central unit of FSA has little impact on the performance of RCS reduction; the FSA serving as a ground plane of the monopole effectively lowers the out-of-band RCS level of the monopole.

For comparison, we also measured a PEC-backed monopole antenna. The ground plane of the single PEC-backed monopole is 50 mm in diameter printed on the underside of a perforated F4B substrate, as shown in the insets of Fig. 22. The substrate for the monopole is 1 mm in thickness. According to Fig. 22, the center frequency of the FSA-backed monopole shifts slightly toward higher frequencies, and the bandwidth narrows, which is a consequence of near-field coupling. In Fig. 23, the scattering and radiation performance of the single PEC-backed monopole is also provided as a reference. From Fig. 22 and Fig. 23, it is clear that our designed band-notched FSA allows the monopole antenna to work properly at the notch-band and maintains its radiation pattern, while at other frequencies, the FSA still works as an absorber, thereby reducing the RCS of the antenna.

For an electrically controlled FSA loaded with varactors, in actual use, we recommend using an analog-digital converter (DAC) to control the bias voltage of the varactor diodes and a microcontroller to control the DAC [27]. In this way, the notch frequency of the FSA can be instantly manipulated by a computer via communication with the microcontroller. The operating frequency of the antenna is correlated with the notch frequency; thus, the RCS of a frequency-sweep antenna can be reduced in real time.

Table II provides a comparison of our two designs with two other reported band-notched FSAs. Only our designs have adjustable and highly selective notches. The tunable range of the electrically controlled FSA is limited by the capacitance range of the varactor diode (MA46H120).

VII. CONCLUSION

In this paper, we presented two ultrawideband FSA designs with a flexibly adjustable and highly selective notch. By cascading a band-stop FSS layer after the resistive layer, a notch is inserted to the wide absorption band, and the notch frequency is fully controlled by the lossless layer, which can be shifted across the entire absorption band by simply adjusting the lossless layer. Less than 0.5 dB insertion loss is realized at notch frequencies. It is expected that the notched absorber can be combined with an antenna or an antenna array and serve as a ground plane or FSS reflector to realize out-of-band RCS reduction.

The notch frequency of the first design is geometrically controlled, which means the notch is adjusted by replacing the lossless layer and can be applied to narrowband antennas. Thanks to the smaller cell size compared to wavelength and the rotationally symmetric structure, this absorber has good angular stability, and is equally effective for both *y*- and *x*-polarization within the incident angle of 30º.

Loading a varactor in the lossless FSS, the notch frequency of the second design is electrically controllable under *y*-polarization, which is better for real-time control of notch frequency, thereby realizing efficient and cost-effective regulation by simply changing the applied voltage of the varactor. Thanks to its real-time control of the notch band, this band-notched absorber can be used not only in narrowband antennas, but also in wideband antennas to create low RCS antennas. A ratio bandwidth (f_{H2}/f_{L1}) of 4:1 is realized for this FSA. Under *x*-polarization, the FSA retains wideband absorption characteristics.

In the final stages of this work, prototypes of the notched absorbers were fabricated and measured. The theoretical analysis, full-wave simulation, ECM, and experimental results were found to be in reasonable agreement, demonstrating the validity of the proposed design strategies. Moreover, an FSA-backed monopole is measured and vividly shows that the two FSAs can serve as antenna's ground plane and reduce RCS of the antenna.

REFERENCES

[1] W. W. Salisbury, "Absorbent body for electromagnetic waves," U.S. Patent 2 599 944. Jun. 10, 1952.

[2] B. Chambers and A. Tennant, "Design of wideband Jaumann radar absorbers with optimum oblique incidence performance," *Electron. Lett.*, vol. 30, no. 18, pp. 1530–1532, Sept. 1994.

[3] O. Bucci and G. Franceschetti, "Scattering from wedge-tapered absorbers," *IEEE Trans. Antennas Propag.*, vol. 19, no. 1, pp. 96–104, Jan. 1971.

[4] B. A. Munk, *Frequency Selective Surfaces: Theory and Design*. New York, NY, USA: Wiley, 2000.

[5] F. Costa and A. Monorchio, "A frequency selective radome with wideband absorbing properties," *IEEE Trans. Antennas Propag.*, vol. 60, no. 6, pp. 2740–2747, Jun. 2012.

[6] Q. Chen, S. Yang, J. Bai, and Y. Fu, "Design of absorptive/transmissive frequency-selective surface based on parallel resonance," *IEEE Trans. Antennas Propag.*, vol. 65, no. 9, pp. 4897–4902, Sept. 2017.

[7] M. Z. Joozdani and M. K. Amirhosseini, "Wideband absorber with combination of plasma and resistive frequency selective surface," *IEEE Trans. Plasma Sci.*, vol. 44, no. 12, pp. 3254–3261, Dec. 2016.

[8] R. Panwar, S. Puthucheri, V. Agarwala, and D. Singh, "Fractal frequency-selective surface embedded thin broadband microwave absorber coatings using heterogeneous composites," *IEEE Trans. Microw. Theory Tech.*, vol. 63, no. 8, pp. 2438–2448, Aug. 2015.

[9] L. Zhang *et al.*, "A broadband radar absorber based on perforated magnetic polymer composites embedded with FSS," *IEEE Trans. Magn.*, vol. 50, no. 5, pp. 1–5, May 2014.

[10] B. A. Munk, *Metamaterials: Critique and Alternatives*. Hoboken, NJ, USA: Wiley, 2009.

[11] S. Zheng, Y. Yin, J. Fan, X. Yang, B. Li, and W. Liu, "Analysis of miniature frequency selective surfaces based on fractal antenna-filter-antenna arrays," *IEEE Antennas Wireless Propag. Lett.*, vol. 11, no. 2, pp. 240–243, Mar. 2012.

[12] Q. Guo, Z. Li, J. Su, Y. Yang, and J. Song, "Dual-polarization absorptive/transmissive frequency selective surface based on tripole elements," *IEEE Antennas Wireless Propag. Lett.*, vol. 18, no. 5, pp. 961–965, May 2019.

[13] H. Huang, Z. Shen, and A. A. Omar, "3-D absorptive frequency selective reflector for antenna radar cross section reduction," *IEEE Trans. Antennas Propag.*, vol. 65, no. 11, pp. 5908–5917, Nov. 2017.

[14] P. Mei, X. Lin, J. Yu, A. Boukarkar, P. Zhang, and Z. Yang, "Development of a low radar cross section antenna with band-notched absorber," *IEEE Trans. Antennas Propag.*, vol. 66, no. 2, pp. 582–589, Feb. 2018.

[15] Q. Chen, D. Sang, M. Guo, and Y. Fu, "Frequency-selective rasorber with interabsorption band transparent window and interdigital resonator," *IEEE Trans. Antennas Propag.*, vol. 66, no. 8, pp. 4105–4114, Aug. 2018.

[16] P. Mei, X. Lin, J. Yu, and P. Zhang, "A band-notched absorber designed with high notch-band-edge selectivity," *IEEE Trans. Antennas Propag.*, vol. 65, no. 7, pp. 3560–3567, Jul. 2017.

[17] X. Lin, P. Mei, P. Zhang, Z. Chen, and Y. Fan, "Development of a resistor-loaded ultrawideband absorber with antenna reciprocity," *IEEE Trans. Antennas Propag.*, vol. 64, no. 11, pp. 4910–4913, Nov. 2016.

[18] S. Ogawa, Y. Takagawa, and M. Kimata, "Fano resonance in asymmetric-period two-dimensional plasmonic absorbers for dual-band uncooled infrared sensors," *Opt. Eng.*, vol. 55, no. 11, p. 117105, Nov. 2016.

[19] A. A. Omar and Z. Shen, "Double-sided parallel-strip line resonator for dual-polarized 3-D frequency-selective structure and absorber," *IEEE Trans. Microw. Theory Tech.*, vol. 65, no. 10, pp. 3744-3752, Oct. 2017.

[20] B. A. Munk, P. Munk, and J. Pryor, "On designing Jaumann and circuit analog absorbers (CA absorbers) for oblique angle of incidence," *IEEE Trans. Antennas Propag.*, vol. 55, no. 1, pp. 186–193, Jan. 2007.

[21] F. Costa, A. Monorchio and G. Manara, "Analysis and design of ultra thin electromagnetic absorbers comprising resistively loaded high impedance surfaces," *IEEE Trans. Antennas Propag.*, vol. 58, no. 5, pp. 1551-1558, May 2010.

[22] E. F. Knott, *Radar Cross Section Measurements, 2nd ed*. New York, NY, USA: Van Nostrand Reinhold, 1993.

[23] D. C. Jenn, *Radar and Laser Cross Section Engineering*. Reston, VA, USA: AIAA, 2005.

[24] L. Gao *et al.*, "Broadband diffusion of terahertz waves by multi-bit coding metasurfaces," *L. Sci. Appl.*, vol. 4, no. 9, Sept. 2015.

[25] W. Chen, C. A. Balanis, and C. R. Birtcher, "Checkerboard EBG surfaces for wideband radar cross section reduction," *IEEE Trans. Antennas Propag.*, vol. 63, no. 6, pp. 2636-2645, Jun. 2015.

[26] S. Li *et al.*, "Ultra-broadband reflective metamaterial with RCS reduction based on polarization convertor, information entropy theory and genetic optimization algorithm," *Sci. Rep.*, vol. 6, no. 37409, pp. 1-12, Nov. 2016.

[27] S. V. Hum, M. Okoniewski and R. J. Davies, "Realizing an electronically tunable reflectarray using varactor diode-tuned elements," *IEEE Microw. Wireless Compon. Lett.*, vol. 15, no. 6, pp. 422-424, Jun. 2005.

[28] Y. Han, L. Zhu, Y. Chang and B. Li, "Dual-polarized bandpass and band-notched frequency-selective absorbers under multimode resonance," *IEEE Trans. Antennas Propag.*, vol. 66, no. 12, pp. 7449-7454, Dec. 2018.

Yuxuan Ding received the B.Eng. degree in communication engineering from Communication University of China, Beijing, China, in 2019. She is currently pursuing the Ph.D. degree in electromagnetic field and microwave technology with National Space Science Center, the University of Chinese Academy of Sciences, Beijing, China.

Her current research interests include metamaterial absorber, low RCS antenna and reflectarray antenna.

Mengyao Li received the B.Eng. degree in communication engineering from Communication University of China, Beijing, China, in 2020.

Her current research interests include the design of metamaterial absorbers and periodic structures.

Jianxun Su received the B.S. degree in Electronic Information Engineering from Taiyuan University of Technology, Taiyuan, China, in 2006; the M.S. degree and the Ph.D. degree in Electromagnetic Field and Microwave Technology from the Communication University of China and Beijing Institute of Technology, Beijing, China, in 2008 and 2011, respectively.

From 2012 to 2014, he was with China Electronics Technology Group Corporation (CETC), where he engaged in phased-array system research. He is currently working as a professor at School of Information Engineering, Communication University of China and also with the Science and Technology on Electromagnetic Scattering Laboratory.

His special research interests include integral equation method, metamaterial, phased-array antenna, radar target characteristics.

Qingxin Guo (M‘11-SM’12) received the B.S., M.S., and Ph.D. degree in electromagnetic field and microwave technology from Communication University of China, Beijing, China, in 1997, 2006 and 2013 respectively.

From 1997 to 2002, He was an engineer of Xiamen Overseas Chinese Electronics Co., Ltd., where he was involved with the repeaters and the mobile phone for the GSM system. From 2002 to 2004, he was a project manager of Beijing Gigamega Electronics Co., Ltd., where he was responsible for the design of amplifier for transmitter. From 2004 to 2008, he was an engineer and a project manager of Beijing Filcom Technology Co. Ltd., where he was responsible for the design of combiner and multiplexer. In 2006, he joined Communication University of China, where he has been an Associate Professor with School of Information Engineering since 2013. From 2011 to 2012, he was a visiting researcher of Electromagnetic Communication laboratory (EMC lab) which is affiliated with Electrical Engineering Department at Pennsylvania State University. His research interests include the antennas, microwave passive components, RF circuits and metamaterial.

Hongcheng Yin was born in Yujiang, Jiangxi, China, in 1967. He received the B.S. degree from the Northwest Telecommunication Engineering Institute, Xi’an, China, in 1986, the M.S. degree from the Science and Technology on Electromagnetic Scattering Laboratory, Beijing, China, in 1989, and the Ph.D. degree from Southeast University, Nanjing, China, in 1993, all in electromagnetic field and microwave technique.

He is currently a Research Scientist with the Science and Technology on Electromagnetic Scattering Laboratory. He has coauthored over three books and published more than 120 papers in technical journals. His current research interests include electromagnetic scattering, radar target signature, and radar target identification.

Dr. Yin is a fellow of the Chinese Institute of Electronics.

Zhengrui Li received the B.S. degree in communication and information system from Beijing Jiaotong University, Beijing, China, in 1984; the M.S. degree in electrical engineering from Beijing Broadcast Institute, Beijing, China, in 1987; and the Ph.D. degree in electrical engineering from Beijing Jiaotong University, Beijing, China, in 2009.

He is currently a Professor with the Communication University of China, Beijing, China. He studied at Yokohama National University, Yokohama, Japan, from 2004 to 2005. His research interests include the areas of finite-difference time-domain (FDTD) methods, electromagnetic scattering, metamaterials and antennas.

Prof. Li is a Senior Member of the Chinese Institute of Electronics.

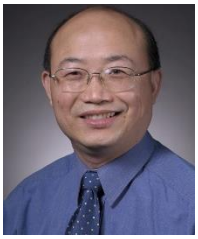

Jiming Song (S’92-M’95-SM’99-F’14) received the B.S. and M.S. degrees in physics from Nanjing University, China, in 1983 and 1988, respectively, and the Ph.D. degree in electrical engineering from Michigan State University, East Lansing, USA in 1993.

From 1993 to 2000, he worked as a Postdoctoral Research Associate, a Research Scientist and Visiting Assistant Professor at the University of Illinois at Urbana-Champaign. From 1996 to 2000, he worked part-time as a Research Scientist at SAIC-DEMACO. Dr. Song was the principal author of the Fast Illinois Solver Code (FISC). He was a Principal Staff Engineer/Scientist at Semiconductor Products Sector of Motorola in Tempe, Arizona before he joined Department of Electrical and Computer Engineering at Iowa State University as an Assistant Professor in 2002.

Dr. Song currently is a Professor at Iowa State University’s Department of Electrical and Computer Engineering, and also a Visiting Professor at the School of Information Engineering, Communication University of China, Beijing, China. His research has dealt with modeling and simulations of interconnects on lossy silicon and RF components, electromagnetic wave scattering using fast algorithms, the wave propagation in metamaterials, acoustic and elastic wave propagation and non-destructive evaluation, and transient electromagnetic field. He was selected as a National Research Council/Air Force Summer Faculty Fellow in 2004 and 2005 and received the NSF Career Award in 2006. Dr. Song is an ACES Fellow, an associate editor for IEEE Antennas and Wireless Propagation Letters (AWPL) and ACES Express.